Full vectorial analysis of Brillouin gain in random acoustically microstructured photonic crystal fibers

Chad G. Carlson, R. Brendan Ross, Jessica M. Schafer, Justin B. Spring, and Benjamin G. Ward
Laser and Optics Research Center, Department of Physics, United States Air Force Academy, 2354 Fairchild Drive Suite 2A31, USAF Academy, Colorado 80840, USA

(Received 9 July 2010; revised manuscript received 17 February 2011; published 7 June 2011)

We report on the fully vectorial numerical investigation of Brillouin gain in large-mode-area random acoustically microstructured photonic crystal fibers. We treated the fiber core as a linear isotropic elastic medium, resulting in an energy functional that we minimized to obtain the heterogeneous, anisotropic, and Stokes-frequency-dependent vector acoustic displacement field used to calculate the Brillouin gain spectra with a finite element method. We found that the peak Brillouin gain is dependent on the size of the acoustic domains and that a 4% spread in acoustic velocities results in peak Brillouin gain values suppressed by 8 dB relative to that of homogeneous fused silica fibers.

DOI: 10.1103/PhysRevB.83.235110 PACS number(s): 42.81.−i, 78.35.+c, 42.65.Es

I. INTRODUCTION

In the single-frequency, high-power operating regime, stimulated Brillouin scattering (SBS) is often the nonlinearity with the lowest threshold in optical fibers.[1,2] SBS is a nonlinear optical process in which an electromagnetic field generates copropogating acoustic phonons through electrostriction. The copropagating phonons act as a moving Bragg grating, backscattering a portion of the optical field. The interference of the two counterpropagating optical fields reinforces the scattering phonon, leading to a positive feedback loop after a certain threshold power is crossed.[3–6] SBS limits the amount of optical output power in a fiber laser or amplifier and can lead to catastrophic optical damage. SBS has been studied extensively for single-mode, multimode, and photonic crystal fibers.[7]

In recent years, significant efforts have been undertaken to mitigate SBS in large-mode-area optical fibers to further power scaling efforts in very-high-power fiber lasers and amplifiers. SBS mitigation techniques include, but are not limited to, applying a longitudinal strain[8] or temperature gradient along the length of the fiber,[9] creating an acoustic guiding layer[10] or a linearly ramped acoustic index,[11] varying the structural properties of a photonic crystal longitudinally to vary the Brillouin shift,[12] and using a nanostructured core to create a phononic band gap.[13] In small-core photonic crystal fibers, experimental results have demonstrated an SBS threshold that is three to five times larger than similar step-index fibers.[14–16] Small-core fibers are unsuitable for high-power propagation though, due to their reduced nonlinear effective area.[17] In each case, the increase in SBS threshold was attributed to acoustic guiding/antiguiding provided by the microstructure of the fiber. In a recent publication, we demonstrated that SBS suppression in a large-mode-area microstructured fiber is possible by a random structuring of different acoustic domains in the core of a photonic crystal fiber.[18]

Due to the high cost in manufacturing microstructured fibers, determination of the optimal microstructure arrangement for maximum SBS suppression prior to manufacture is critical. Simulation of SBS in optical fibers often relies on solving a scalar form of the acoustic wave equation for the longitudinal acoustic displacement, which is primarily responsible for the onset and evolution of SBS.[19] Such an approximation is well suited for fibers that have a homogeneous acoustic index and azimuthal symmetry. SBS in fibers with arbitrary radial index profiles has been considered in a two-dimensional model,[20] which demonstrated that neglect of radial motion had a significant effect on the Brillouin gain spectrum. Asymmetry in photonic crystal fibers together with discontinuous optical profiles caused by glass/air interfaces naturally suggests a finite element approach. Simulation of the Brillouin gain spectrum of photonic crystal fibers with arbitrary acoustic designs suitable for SBS suppression demands a fully vectorial model of the acoustic displacement.

A fully vectorial method has been reported previously in the literature,[13] but this previous model did not include the effects of electrostriction. The model presented here includes electrostriction, enabling a study of the phonon decay rate, the finite width of the Brillouin gain spectrum, and photon-phonon coupling mechanisms. In this paper, we analyze the Brillouin gain of photonic crystal fibers that have regions of constant acoustic index randomly assigned across the core, using a fully vectorial finite element model. We will demonstrate that the size and shape of these acoustic domains can be varied to tailor the SBS spectrum, leading to an 8 dB increase in the SBS threshold for optimally sized acoustic domains in a large-mode-area photonic crystal fiber.

II. THEORY

The analysis of the SBS process begins with the nonhomogeneous optical wave equation

$$\nabla \times \nabla \times \vec{E} - \frac{n^2\omega^2}{c^2}\vec{E} = \vec{P}_{NL}, \tag{1}$$

where $\vec{E}$ is the electric field, n is the index of refraction, ω is the optical frequency, c is the speed of light, and $\vec{P}_{NL}$ is the nonlinear polarization driving term. The nonlinear polarization is caused by electrostriction, and can be expressed as

$$\begin{aligned} P_{NLi} &= -n^4\varepsilon_0 p_{ijrs}\epsilon_{rs}E_j \\ &= -\gamma_{12}(\nabla\cdot\vec{u})E_i - 2\gamma_{44}(\nabla_s\vec{u})_{ij}E_j \end{aligned} \tag{2}$$

where p is the strain optic tensor and ϵ is the strain,[21,22]

$$(\nabla_s \vec{u})_{ij} \equiv \frac{1}{2}\left(\frac{\partial u_i}{\partial x_j} + \frac{\partial u_j}{\partial x_i}\right) \tag{3}$$

is the symmetric part of the displacement gradient, and the electrostrictive constants take the value $\gamma_{ij} = n^4 \varepsilon_0 p_{ij}$, where ε_0 is the vacuum permittivity and p_{ij} are the strain optic tensor components. Given a known electric field inside the fiber, one can find $\vec{u}$ by solving the nonhomogeneous acoustic wave equation[22]

$$\rho \frac{\partial^2 \vec{u}}{\partial t^2} = \nabla \cdot \left[\overleftrightarrow{c} : (\nabla_s \vec{u}) + \overleftrightarrow{\eta} : \frac{\partial (\nabla_s \vec{u})}{\partial t} \right] + \frac{1}{2} \overleftrightarrow{\gamma} : (\vec{E} \otimes \vec{E}), \tag{4}$$

where ρ is the mass density, $\overleftrightarrow{c}$ is the elastic stiffness tensor, $\overleftrightarrow{\eta}$ is the viscosity tensor, and $\overleftrightarrow{\gamma}$ is the electrostrictive tensor, : represents tensor contraction in two indices, and $\otimes$ denotes the outer product. Fused silica is an isotropic material so each of these rank-4 tensors may be expressed in terms of two constants, allowing considerable simplification of (4) and yielding[22]

$$\left[\rho v_\ell^2 + \eta_{11} \frac{\partial}{\partial t}\right] \nabla(\nabla \cdot \vec{u}) - \left[\rho v_t^2 + \eta_{44} \frac{\partial}{\partial t}\right] \nabla \times \nabla \times \vec{u} - \rho \frac{\partial^2 \vec{u}}{\partial t^2} = -\frac{\gamma_{12}}{2} \nabla \mid E \mid^2 - \gamma_{44} \nabla \cdot (\vec{E} \otimes \vec{E}), \tag{5}$$

where $v_{\ell,t}$ are the longitudinal and transverse acoustic velocities given by $v_\ell^2 = c_{11}/\rho$ and $v_t^2 = c_{44}/\rho$, respectively, η_{11} and η_{44} are the viscoelastic constants for longitudinal and transverse acoustic waves, respectively, and γ_{12} and γ_{44} are defined as before. Although each of these physical properties can vary throughout the fiber due to glass composition variations, we restrict our treatment to the case where only the acoustic velocities are heterogeneous and do not distinguish between the effects of the mass density and the elastic constants on these velocity variations. Hence, we take ρ, η_{11}, η_{44}, γ_{12}, and γ_{44} to be constant throughout the fiber.

Using the identity $\nabla(\nabla \cdot \vec{u}) = \nabla \times \nabla \times \vec{u} + \nabla^2 \vec{u}$ to eliminate the term containing the divergence and assuming harmonically varying fields so that $\partial \vec{u}/\partial t = i\Omega \vec{u}$, we obtain

$$\left[\rho\left(v_\ell^2 - v_t^2\right) + i\Omega\left(\eta_{11} - \eta_{44}\right)\right] \nabla \times \nabla \times \vec{u} + \left[\rho v_\ell^2 + i\Omega \eta_{11}\right] \nabla^2 \vec{u} + \rho \Omega^2 \vec{u} = -\frac{\gamma_{12}}{2} \nabla \mid E \mid^2 - \gamma_{44} \nabla \cdot (\vec{E} \otimes \vec{E}). \tag{6}$$

According to the principle of least action, the acoustic wave equation (6) may be obtained by minimizing a suitable variational form. The electromagnetic wave equation[23] and Poisson's equation[24] together contain terms of the same forms as those in (6). Invoking the derivations contained in these last two references leads to the form

$$S\{\vec{u}\} = \iint s\left[\vec{u}(\vec{r},t)\right] dA, \tag{7a}$$

$$s[\vec{u}(\vec{r},t)] = -\frac{1}{2}\left[v_\ell^2(\vec{r}) + i\Omega \frac{\eta_{11}}{\rho}\right] |\nabla \vec{u}(\vec{r})|^2 - \frac{1}{2}\left[v_\ell^2(\vec{r}) - v_t^2(\vec{r}) + i\Omega \frac{(\eta_{11} - \eta_{44})}{\rho}\right] \cdot |\nabla \times \vec{u}(\vec{r})|^2 + \frac{1}{2}\Omega^2 |\vec{u}(\vec{r})|^2 + \vec{F}(\vec{r}) \cdot \vec{u}(\vec{r}), \tag{7b}$$

$$\vec{F}(\vec{r}) = \frac{\gamma_{12}}{2\rho}[\nabla |E(\vec{r})|^2] + \frac{\gamma_{44}}{\rho}[\nabla \cdot (\vec{E}(\vec{r}) \otimes \vec{E}(\vec{r}))]. \tag{7c}$$

Note that the signs of the first two terms of (7b) change when we take the functional derivative of this expression with respect to $\vec{u}$ to obtain (6). Furthermore, division of both sides of (6) by a uniform value of ρ is justified because the spatial variation of the driving term is dominated by the electromagnetic contribution, which approaches zero at the boundary of the core region. The domain of integration in (7a) is the fiber cross section. In order for Brillouin gain to occur, the optical and acoustic waves described by (1) and (5) must be phase matched. In the slowly varying envelope approximation, in the absence of pump depletion, with the pump wave traveling in the positive z direction, we have

$$\vec{E}_p = \frac{1}{2}[a_p \vec{f}(x,y) \exp[-i(k_p z - \omega_p t)] + \text{c.c.}], \tag{8a}$$

$$\vec{E}_s = \frac{1}{2}[a_s(z) \vec{f}(x,y) \exp[i(k_s z + \omega_s t)] + \text{c.c.}], \tag{8b}$$

$$\vec{u} = \frac{1}{2}[\vec{\phi}(x,y) \exp[-i(\beta z - \Omega_t)] + \text{c.c.}], \tag{8c}$$

where c.c. denotes the complex conjugate. The phase-matching conditions are then $\beta = k_p + k_s$ and $\Omega = \omega_p - \omega_s$. To make use of (8) we enumerate the derivative terms in (7b):

$$|\nabla \vec{u}(\vec{r})|^2 = \frac{\partial u_i^*}{\partial x_j} \frac{\partial u_i}{\partial x_j}, \tag{9a}$$

$$|\nabla \times \vec{u}(\vec{r})|^2 = \varepsilon_{ijk} \varepsilon_{ilm} \frac{\partial u_j^*}{\partial x_k} \frac{\partial u_l}{\partial x_m}, \tag{9b}$$

where ε_{ijk} is the Levi-Cività symbol, and then substitute

$$\frac{\partial u_i}{\partial x} = \frac{1}{2}\left[\frac{\partial \phi_i(x,y)}{\partial x} \exp\left[-i(\beta z - \Omega t)\right] + \text{c.c.}\right], \tag{10a}$$

$$\frac{\partial u_i}{\partial y} = \frac{1}{2}\left[\frac{\partial \phi_i(x,y)}{\partial y} \exp\left[-i(\beta z - \Omega t)\right] + \text{c.c.}\right], \tag{10b}$$

$$\frac{\partial u_i}{\partial z} = \frac{1}{2}\left[-i\beta \phi_i(x,y) \exp\left[-i(\beta z - \Omega t)\right] + \text{c.c.}\right]. \tag{10c}$$

We also carry out the same procedure for the terms containing the derivatives of $\vec{E}$. Removing the non-phase-matched terms, canceling out the oscillatory dependence of the remaining phase-matched terms, and inserting the field distribution $\vec{f}$ characterizing the fundamental mode of the optical waveguide, we obtain a time-independent variational form that is a functional of $\vec{\phi}(x,y)$:

$$\tilde{S}\{\vec{\phi}\} = \iint \tilde{s}[\vec{\phi}(x,y)] dA. \tag{11}$$

We find no suitable analytic method for minimizing this functional for arbitrary spatially dependent material v_ℓ and v_t so we resort to a finite element scheme which treats discontinuities in material properties naturally. We thus introduce vectors $\mathbf{U}$ and $\mathbf{F}$ that define the values of $\vec{\phi}$ and the electrostrictive driving function $\vec{F}(\vec{r})$ on the nodes of the finite element mesh. For a mesh with N nodes, $\mathbf{U}$ and $\mathbf{F}$ each have $3N$ entries to specify each component of $\vec{\phi}$ and $\vec{F}(\vec{r})$ on each node.

These vectors are subdivided into vectors corresponding to each component as

$$\mathbf{U} = [\,\mathbf{U}_x\ \mathbf{U}_y\ \mathbf{U}_z\,],\quad \mathbf{F} = [\,\mathbf{F}_x\ \mathbf{F}_y\ \mathbf{F}_z\,]. \tag{12}$$

We approximate the integral in (7a) by interpolating the values of the fields and their derivatives at integration points within the interior of the elements from their values at the nodes given by $\mathbf{U}$ and $\mathbf{F}$, performing a weighted sum over the integration points, and summing over all of the elements in the mesh. We approximate the acoustic velocities of the fiber v_t and v_ℓ to be uniform within each element.

Shape function matrices $\mathbf{N}_k$, $\mathbf{N}_{xk}$, and $\mathbf{N}_{yk}$ accomplish the interpolation of the values $\mathbf{U}_i$ at the nodes to values and derivatives at integration points k for all elements simultaneously:[19]

$$\tilde{\mathbf{U}}_{ik} = \mathbf{N}_k \cdot \mathbf{U}_i^T, \tag{13a}$$

$$\frac{\partial \tilde{\mathbf{U}}_{ik}}{\partial x_j} = \mathbf{N}_{jk} \cdot \mathbf{U}_i^T, \tag{13b}$$

where the shape function matrices have dimension $M \times N$, M being the number of elements, and T denotes the transpose of the matrix. Additionally, we construct diagonal $M \times M$ matrices $\mathbf{V}_L^2$ and $\mathbf{V}_T^2$ containing the squared longitudinal and transverse acoustic velocities within each element on the diagonal and $\mathbf{J}_k$ containing the Jacobian matrix for the local to global coordinate transformation at integration points k for each element also on the diagonal. These matrices facilitate integration of the terms in the variational form (11).

For example, the term proportional to Ω^2 is

$$\begin{aligned}\tilde{S}\{\vec{\phi}\}_{\Omega^2} &= \frac{1}{2}\Omega^2 \int\!\!\int \vec{\phi}^*(x,y)\cdot\vec{\phi}(x,y)dA \\ &\approx \frac{1}{2}\Omega^2 \sum_{k=1}^{7} W_k \tilde{\mathbf{U}}_{xk}^T \cdot \mathbf{J}_k \cdot \tilde{\mathbf{U}}_{xk} \\ &\quad + \frac{1}{2}\Omega^2 \sum_{k=1}^{7} W_k \tilde{\mathbf{U}}_{yk}^T \cdot \mathbf{J}_k \cdot \tilde{\mathbf{U}}_{yk} \\ &\quad + \frac{1}{2}\Omega^2 \sum_{k=1}^{7} W_k \tilde{\mathbf{U}}_{zk}^T \cdot \mathbf{J}_k \cdot \tilde{\mathbf{U}}_{zk},\end{aligned} \tag{14}$$

where W_k are the integration point weights. Use of (12) and (13) allows us to write this as

$$\tilde{S}\{\vec{\phi}\}_{\Omega^2} \approx S(\mathbf{U})_{\Omega^2} \equiv -\frac{1}{2}\Omega^2 \mathbf{U}\cdot\mathbf{C}\cdot\mathbf{U}^T, \tag{15}$$

where

$$\mathbf{C} = \begin{pmatrix} \mathbf{C}_{xx} & 0 & 0 \\ 0 & \mathbf{C}_{yy} & 0 \\ 0 & 0 & \mathbf{C}_{zz} \end{pmatrix} \tag{16}$$

is then a $3N \times 3N$ matrix and

$$\mathbf{C}_{xx} \equiv \mathbf{C}_{yy} \equiv \mathbf{C}_{zz} \equiv -\sum_{k=1}^{7} W_k \left[\mathbf{N}_k^{\mathrm{T}} \cdot \mathbf{J}_k \cdot \mathbf{N}_k\right] \tag{17}$$

are each $N \times N$ matrices. Carrying out this procedure for each of the remaining terms and grouping them by powers of Ω, we obtain

$$S(\mathbf{U}) = \tfrac{1}{2}\mathbf{U}^* \cdot [\mathbf{A} + \Omega\mathbf{B} + \Omega^2\mathbf{C}] \cdot \mathbf{U}^T + \mathbf{U}^* \cdot \mathbf{F}^T, \tag{18}$$

where

$$\mathbf{A} = \begin{pmatrix} \mathbf{A}_{xx} & \mathbf{A}_{xy} & \mathbf{A}_{xz} \\ \mathbf{A}_{xy} & \mathbf{A}_{yy} & \mathbf{A}_{yz} \\ \mathbf{A}_{xz} & \mathbf{A}_{yz} & \mathbf{A}_{zz} \end{pmatrix}, \tag{19a}$$

$$\mathbf{B} = \begin{pmatrix} \mathbf{B}_{xx} & \mathbf{B}_{xy} & \mathbf{B}_{xz} \\ \mathbf{B}_{xy} & \mathbf{B}_{yy} & \mathbf{B}_{yz} \\ \mathbf{B}_{xz} & \mathbf{B}_{yz} & \mathbf{B}_{zz} \end{pmatrix}. \tag{19b}$$

Each submatrix in $\mathbf{A}_{ij}$, $\mathbf{B}_{ij}$, and $\mathbf{C}_{ij}$ is an $N \times N$ matrix. Expressions for these as well as $\mathbf{F}$ are given in the Appendix. The vector $\mathbf{F}$ is derived from the electric field vector which is expressed in terms of hybrid edge nodal elements; hence hybrid shape functions[25] are employed to interpolate the field values and their derivatives onto the integration points. Note that matrices $\mathbf{A}$ and $\mathbf{B}$ are symmetric but $\mathbf{B}$ has complex values and is not Hermitian. The complex entries in $\mathbf{B}$ causes the destruction of phonons, while the source term $\mathbf{F}$ creates phonons. Further details regarding the finite element method are described in a prior publication.[19]

Use of (18) to minimize $\tilde{S}$ with respect to $\mathbf{U}$ yields

$$[\mathbf{A} + \Omega\mathbf{B} + \Omega^2\mathbf{C}]\mathbf{U}^T + \mathbf{F}^T = 0, \tag{20}$$

a linear matrix equation which may be solved to find $\mathbf{U}$ for a given Brillouin frequency shift Ω. We note that this procedure is the discrete counterpart to employment of a Green's function to obtain the vector acoustic displacement profile in the continuous case.[19] We further note that (20) is similar to the equation governing a driven and damped ensemble of coupled oscillators.[26]

Once $\mathbf{U}$ has been found, it may be incorporated into (1) and (2) to obtain the equations describing Brillouin amplification. To do this we note that the index of refraction is uniform within the core of the fiber and the net charge density is zero so that $\nabla\cdot\vec{D} = n^2\nabla\cdot\vec{E} = 0$, where $\vec{D}$ is the electric displacement. The optical wave equation then becomes

$$\nabla^2\vec{E} + \frac{n^2\omega^2}{c^2}\vec{E} = -\vec{P}_{\mathrm{NL}}. \tag{21}$$

Substituting (10) into (21), neglecting the small terms containing $\partial^2 a_s(z)/\partial z^2$, and keeping only the phase-matched terms of the nonlinear polarization[17,27] results in a differential equation for the evolution of the Stokes field along the negative z axis:

$$ik_s\vec{f}\frac{\partial a_s}{\partial z} = \overleftrightarrow{\delta\varepsilon}\cdot\vec{f}, \tag{22}$$

where

$$\overleftrightarrow{\delta\varepsilon} = \frac{\gamma_{12}}{2}\left[\frac{\partial\phi_x}{\partial x} + \frac{\partial\phi_y}{\partial y} + i\beta\phi_z\right]\delta_{ij} + \gamma_{44}\begin{pmatrix} \frac{\partial\phi_x}{\partial x} & \frac{1}{2}\left[\frac{\partial\phi_x}{\partial y} + \frac{\partial\phi_y}{\partial x}\right] & \frac{1}{2}\left[i\beta\phi_x + \frac{\partial\phi_z}{\partial x}\right] \\ \frac{1}{2}\left[\frac{\partial\phi_x}{\partial y} + \frac{\partial\phi_y}{\partial x}\right] & \frac{\partial\phi_y}{\partial y} & \frac{1}{2}\left[i\beta\phi_y + \frac{\partial\phi_z}{\partial y}\right] \\ \frac{1}{2}\left[i\beta\phi_x + \frac{\partial\phi_z}{\partial x}\right] & \frac{1}{2}\left[i\beta\phi_y + \frac{\partial\phi_z}{\partial y}\right] & i\beta\phi_z \end{pmatrix}. \tag{23}$$

Multiplication of both sides by $\vec{f}$ and integration over the fiber cross section, noting that the normalization of the electric field distribution characterizing the guided fiber modes, results in an equation for the evolution of the Stokes amplitude:

$$\frac{\partial a_s}{\partial z} = \frac{1}{ik_s}\iint \vec{f}\cdot\overleftrightarrow{\delta\varepsilon}\cdot\vec{f}\,dA. \tag{24}$$

Application of the expression for optical power

$$P_{s,p} = \frac{1}{2}cn\varepsilon_0|a_{s,p}|^2\iint|\vec{f}(x,y)|^2\,dA \tag{25}$$

yields the equations for the evolution of the Stokes power:

$$-\frac{dP_s(z)}{dz} = \frac{g_B}{A_{\text{eff}}}P_sP_p, \tag{26a}$$

$$\frac{g_B}{A_{\text{eff}}} = \left(\frac{\pi n^2 p_{12}}{2\rho c\varepsilon_0\lambda}\right)\frac{\iint\vec{f}\cdot\overleftrightarrow{\delta\varepsilon}\cdot\vec{f}\,dA}{(\iint|\vec{f}|^2\,dA)^2}, \tag{26b}$$

where $P_{p,s}$ are the forward and counterpropagating pump and Stokes powers, respectively. We note that the coefficients γ_{44}, η_{11}, and η_{44} influence the Brillouin gain coefficient g_B through $\overleftrightarrow{\delta\varepsilon}$. The integrals in (26b) are approximated using the same finite element mesh used to solve the acoustic wave equation. The electric field distribution $\vec{f}$ is determined by a hybrid linear tangential quadratic normal finite element solution to the vector optical wave equation in the absence of a nonlinear polarization.[25] We note that in the plane wave approximation for the acoustic displacement fields, the integral factor in (26b) becomes $\rho\gamma_{12}/(\eta_{11}\Omega)$ so that the usual expression for the peak Brillouin coefficient,[17]

$$g_B = \frac{2\pi^2 n^7 p_{12}^2}{c\lambda^2\rho v_\ell\Gamma}, \tag{27}$$

is recovered, where Γ is the thermal Brillouin linewidth and we have used the relations $\gamma_{12} = n^4\varepsilon_0 p_{12}$, $\Gamma = \beta^2\eta_{11}/\rho$, $v_\ell \approx \Omega/\beta$, and $\beta \approx 4\pi n/\lambda$.

The direct solution of the nonhomogeneous acoustic wave equation (5) eliminates the need to calculate the acoustic modes. Many previous models[19] used the scalar form of (5), taking the divergence of both sides and solving for just the longitudinal acoustic displacement. This approximation is valid for cores with an acoustic index that is homogeneous or slowly varying, but it breaks down for the acoustically microstructured cores considered here. Calculations of the Brillouin gain in axially symmetric fibers including radial but not azimuthal displacements have been accomplished previously.[20] Accurate prediction of the behavior of fibers with arbitrary acoustic designs requires a fully vectorial model that tracks all three components of the acoustic displacement. While a fully vectorial method has been described previously,[13] this work ignored the effect of electrostriction. The present work includes the effect of electrostriction, essential to accurate modeling of the phonon decay rate and the finite width of the Brillouin gain spectrum. Our model has been checked in the limiting case described in Ref. 20 and found to agree with the results presented in that work for the Brillouin gain spectrum of a nonzero-dispersion fiber. Additionally, our model has been checked in the case of a highly doped germanosilicate fiber and found to agree with experimental results obtained for this fiber.[28] Furthermore, (26) reduces to the well-known expression for Brillouin gain in the optically and acoustically homogeneous case.[3–6] In summary, the fully vectorial model described here includes all three components of the acoustic displacement and includes the effects of electrostriction, which allows it to capture the behavior of fibers with arbitrary acoustic designs, including the randomly microstructured cores analyzed below.

III. Fiber Properties

We investigate large-mode-area photonic crystal fiber designs that are optically similar to those previously reported.[29] The core is formed by incorporating seven solid rods within a close-packed triangular lattice of capillary rods within the fiber preform. The lattice pitch is 12 μm and the air hole size is 2.16 μm, corresponding to a diameter to pitch ratio (d/Λ) of 0.18. This optical profile produces a near-Gaussian linearly polarized fundamental mode field profile with a nonlinear effective area of 800 μm^2. The fiber structure and mode field intensity profile are shown in Fig. 1. Although the fiber designs considered have a large mode area, each is designed to operate in a single transverse optical mode regardless of their acoustic properties. Such designs have exhibited single-transverse-mode output at wavelengths near 1.1 μm.[29]

The acoustic velocities within the cladding, comprised of the air-hole lattice, are taken to be those of isotropic bulk silica characterized by a mass density of 2200 kg/m^3, a Young's modulus of 73 GPa, and a Poisson ratio of 0.17, yielding a longitudinal acoustic velocity of 5972 m/s and a shear acoustic velocity of 3766 m/s. The acoustic velocities within the core are defined to be uniform within defined acoustic domains, but different among the domains. We study fibers with four different acoustic velocities that are 0.98, 0.99, 1.00, and 1.01 times those of bulk silica. Different velocity domains may be created by incorporating varying concentrations of different dopants within the rods comprising the core in the preform.[11]

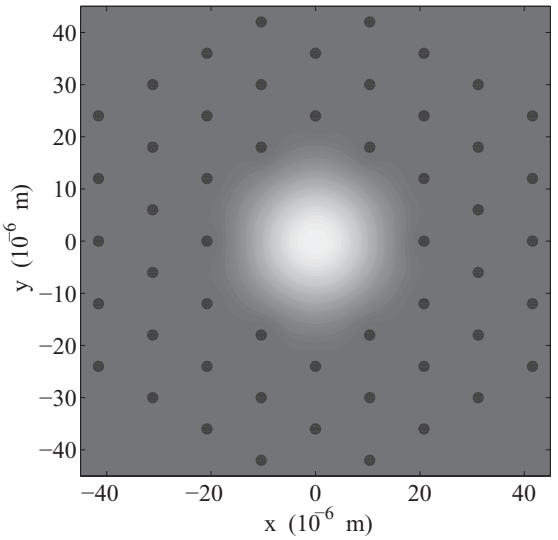

FIG. 1. An illustration of the structural profile and calculated fundamental mode optical intensity profile of the photonic crystal fibers investigated here. The mode profile is plotted with arbitrary units.

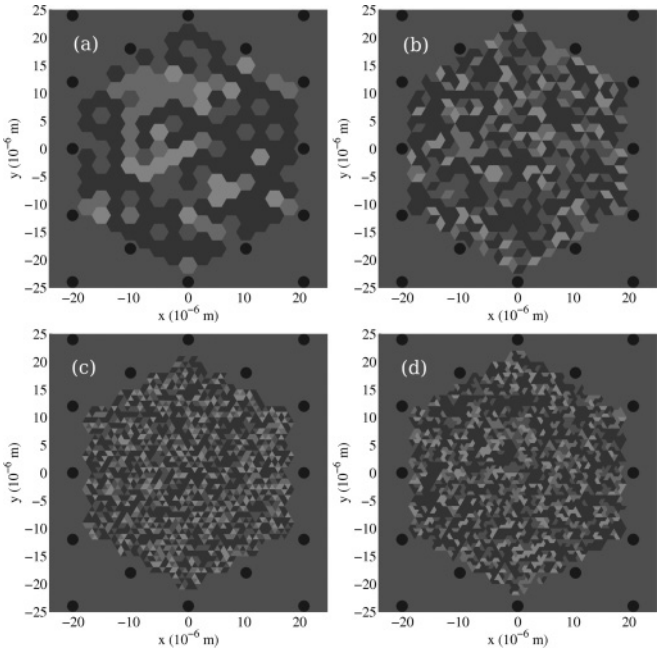

FIG. 2. Samples of random acoustic fibers with different domain sizes and shapes. The darker and ligher regions have higher and lower local acoustic velocities, respectively. There are four different shades within the core region. From darkest to lightest the longitudinal velocities are $1.01v_{\ell 0}$, $1.00v_{\ell 0}$, $0.99v_{\ell 0}$, and $0.98v_{\ell 0}$, where $v_{\ell 0} = 5972$ m/s is the longitudinal acoustic velocity of pure fused silica.

The acoustic domain size will depend on details of the glass processing procedure applied to the core material. The Poisson ratio is assumed to be constant among the domains.

We model the acoustic domains as uniform contiguous subsets of elements within the finite element mesh used to solve the acoustic and optical wave equations governing the Brillouin gain process. By varying the scaling factor $s \equiv \Lambda/\Lambda_c$ between the photonic crystal lattice pitch Λ and the finite element mesh cell pitch Λ_c, we are able to create various different domain shapes with nearly the same sizes. For example, Fig. 2(c), depicting a scaling factor of 2 with one -element domains, and Fig. 2(d), depicting a scaling factor of 3 with three-element domains, have nearly the same domain sizes.

We employed three different scaling factors with five different domain shapes to obtain 15 different variations. For each variation we investigated five different random realizations for a total of 75 configurations.

We have shown in a prior work that, in the scalar acoustic approximation, incorporating a nonuniform acoustic velocity population distribution within the core can enhance Brillouin gain suppression.[18] In particular, more domains with the higher acoustic velocities must be present. To accomplish this, we have defined a probability exponent α such that the probability P_i of a given domain having acoustic velocity i with $i \in \{1, \ldots, 4\}$ arranged from slowest to fastest is given by

$$P_i = 1 - \int_{(i-1)/4}^{i/4} \frac{1}{\alpha} x^{(1-\alpha)/\alpha}\, dx. \tag{28}$$

We have found that the value of $\alpha = 2$ yields the most Brillouin gain suppression; therefore this value is used to obtain all of the results reported here.

IV. RESULTS

We are primarily concerned with the mean value and standard deviation of the peak Brillouin gain coefficient as a function of domain size for different random fiber realizations. Figure 3 shows these values as a function of domain size and comprises the main result of this work. For plotting purposes, we have defined the acoustic domain size as the square root of the acoustic domain area. For comparison, the peak Brillouin gain coefficient for an acoustically homogeneous realization of the fiber is 1.9×10^{-11} m/W. Thus the fibers with an acoustic domain size between approximately 1 and 2 μm exhibit a peak Brillouin gain suppression of approximately 8 dB. This length scale is approximately one to two times the optical wavelength of 1.064 μm and correspondingly two to four times the longitudinal acoustic wavelength. Figure 4 shows the Brillouin gain coefficient values calculated using a scalar approximation[19] for comparison.

The use of different scaling factors s provides assurance that the results are independent of the resolution of the finite element mesh. For example, the two lowest mean g_B values were obtained with element areas of 0.58 and 0.14 μm^2 as were the third- and fourth-highest values on the large-domain side as shown in Fig. 3. Since the domain sizes are comparable in each of these cases, they should have similar mean g_B values. If they did not, this would indicate that the mesh resolution was affecting the g_B values. The fact that all results exhibit the same relationship between domain size and peak g_B value independent of the meshing resolution further confirms its suitability. As an additional check, we doubled the mesh

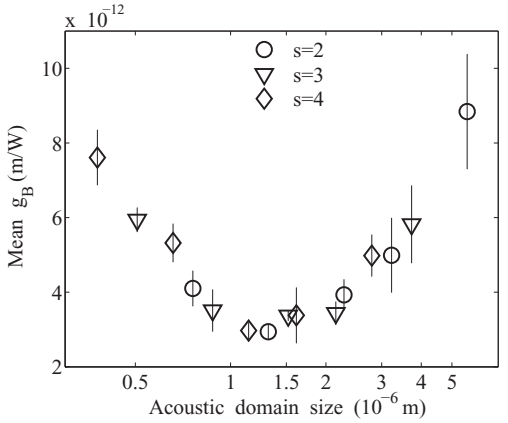

FIG. 3. Peak Brillouin gain coefficient calculated with the fully vectorial model as a function of acoustic domain size. The error bars represent the standard deviations of the values obtained for five different random realizations.

resolution for the realizations of the fiber exhibiting high acoustic transverse spatial frequencies in Fig. 6 and found less than 1% change in the peak g_B values.

The Brillouin gain coefficient for each fiber realization was evaluated at 200 equally spaced Stokes frequencies between 15.8 and 16.8 GHz. The resulting Brillouin gain spectra for a sample random realization of the largest, smallest, and optimum domain sizes are shown in Fig. 5. For the largest domain size, each acoustic domain is able to respond individually at its local Brillouin frequency, resulting in an identifiable peak corresponding to each of the four acoustic velocities. For the smallest domain size, the acoustic wavelength is too large to fully resolve the individual domains and so the acoustic displacements respond to the electrostrictive driving force with an average effective acoustic velocity resulting in a single peak at an intermediate frequency. Neither of these conditions applies to the optimal case which exhibits a broad, flat Brillouin gain spectrum with a correspondingly lower peak value. The domains are small enough that strong resonance in one domain

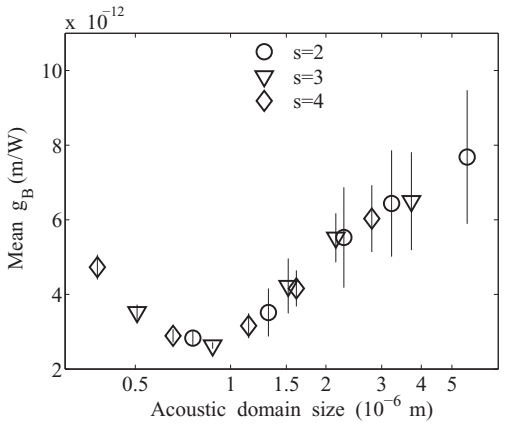

FIG. 4. Peak Brillouin gain coefficient calculated with the scalar model as a function of acoustic domain size. The error bars represent the standard deviations of the values obtained for five different random realizations.

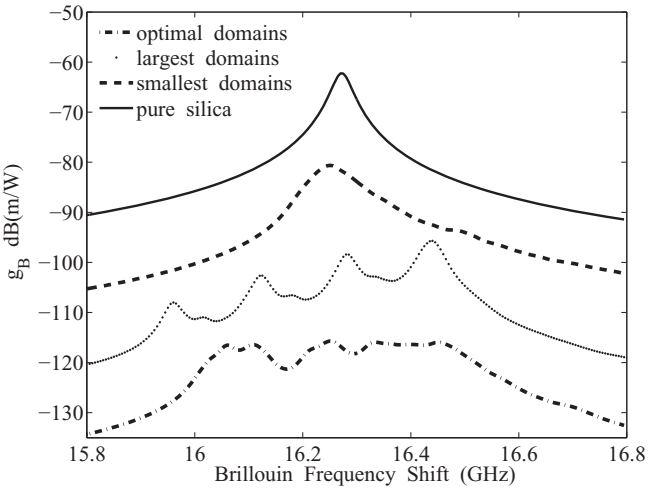

FIG. 5. Brillouin gain spectra of a fiber with the largest domains, a fiber with the smallest domains, a fiber with the optimal domain size, and a fiber with a core of pure silica. Shifts of 15, 30, and 45 dB have been added to the largest domain, smallest domain, and pure silica spectra for readability.

can propagate through neighboring domains and at the same time are large enough to respond electrostrictively at their local resonant frequencies to prevent the spectrum from becoming too narrow.

Examination of the vector acoustic displacement fields for these three cases at the peak Brillouin gain frequency, shown in Fig. 6, reinforces this interpretation. In the case of the large acoustic domains, the peak Brillouin gain frequency corresponds to the local Brillouin frequency of the domains with the highest acoustic velocity. We see that these domains provide a fairly uniform response while the domains with a slower acoustic velocities are driven to respond with a higher spatial frequency, indicating resonance with higher-order acoustic modes. This indicates that if the frequency of a higher-order mode in a slow acoustic domain coincides with a lower-order mode in a fast acoustic domain, they may both contribute to the Brillouin gain at a given frequency, resulting in a higher peak value. We also note that the domains with relatively uniform longitudinal response (corresponding to the z component of the acoustic displacement field) have almost zero transverse response. This provides evidence that the scalar approximation for the acoustic displacement field may be valid for fibers with large acoustic domain sizes.

Comparing the acoustic field profiles of the optimal- and small-domain-size cases, we note that in the optimal case, the longitudinal displacement assumes both positive and negative values while for the small domain size, the longitudinal displacement assumes only positive values. This can be seen by observing that the acoustic field profiles approach zero at the boundary of the plotting domain. The uniform direction of the response in the small-domain case is characteristically similar to the homogeneous acoustic velocity case in which the entire core responds uniformly. This supports the interpretation that as the domain size decreases, the core begins to behave like a homogeneous one with an average intermediate Brillouin

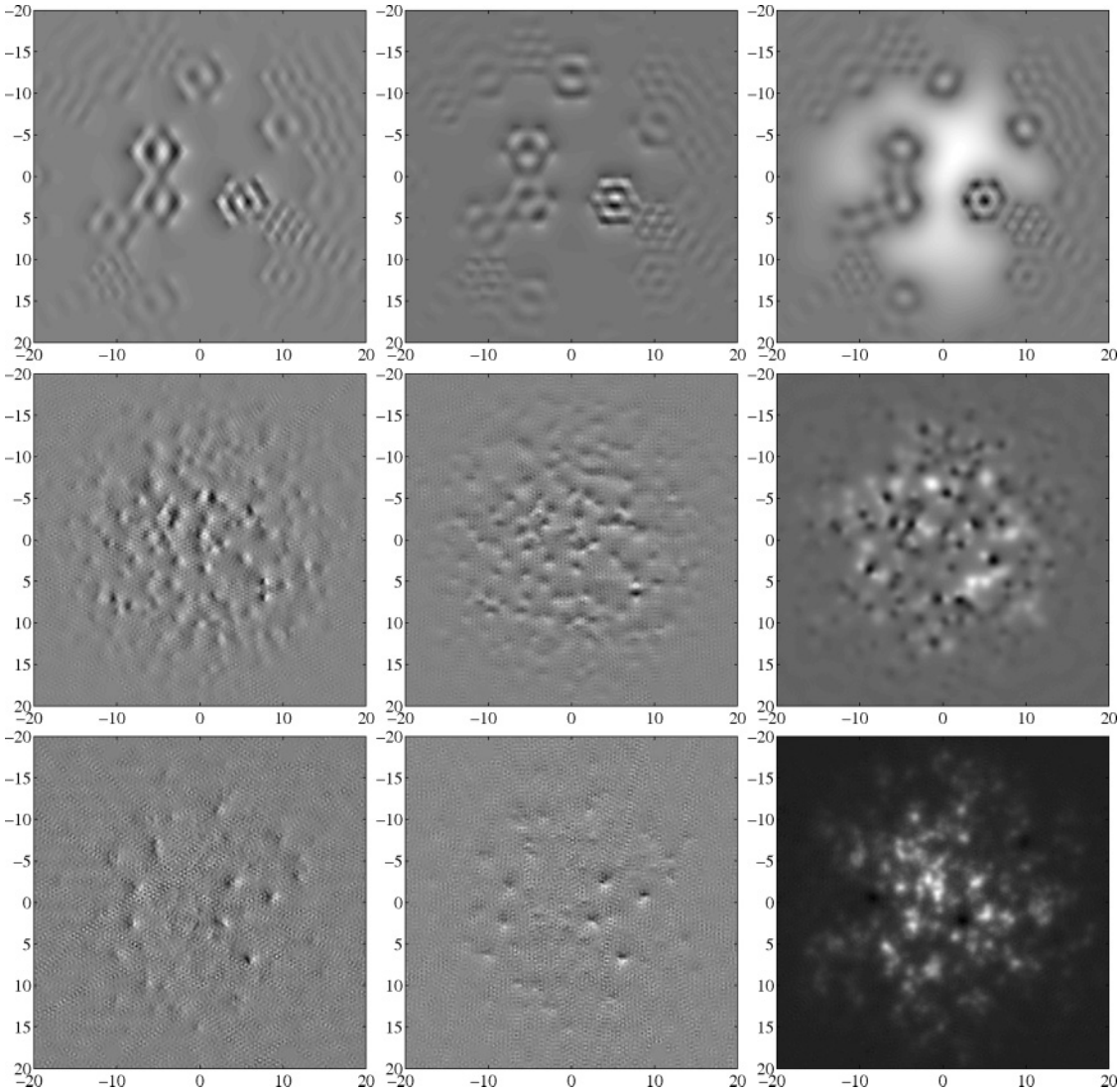

FIG. 6. *x* (first column), *y* (second column), and *z* (third column) components of the acoustic displacement field for the largest (top row), optimal (middle row), and smallest domain size (bottom row) at Brillouin shift frequencies of 16.44, 16.37, and 16.25 GHz respectively. The displacement fields are represented by an arbitrary gray scale level and the units of all axes are micrometers.

peak frequency. Even for the smallest size investigated here, the Brillouin gain spectrum is still considerably broadened at a full width at half maximum of 100 MHz relative to the linewidth of bulk fused silica at this wavelength, which is 36 MHz.[30]

Comparison of the results of the fully vectorial model to the results obtained with a scalar model[18,19] reveals that the scalar model predicts a smaller optimal domain size and fails to predict the rapid onset of larger Brillouin gain values as the domain size is lowered, as the vector model does. This is consistent with the assertion that the fully vectorial treatment is required for fibers with rapid spatial variations in the acoustic velocity. The best agreement between the scalar and vector models is obtained for the largest domain size, consistent with the assertion that the scalar model is suitable with slower spatial variations in the acoustic velocity. Finally, both models predict approximately the same minimum Brillouin gain value.

V. CONCLUSION

Random acoustically microstructured photonic crystal fibers may constitute a method to propagate or amplify high-power single-frequency signals because their reduced Brillouin gain makes their realization a significant potential technical advance. The mathematical description of the Brillouin gain process in such fibers requires retaining the full three-dimensional electromagnetic and acoustic fields in the acoustic and optical wave equations. We have presented a fully vectorial finite element method for calculating the Brillouin gain spectrum in these fibers as well as any other optically and acoustically heterogeneous fiber lacking azimuthal symmetry. This method has been verified against published results for several limiting cases. We have found that for technically feasible material parameters and waveguide geometry, random acoustically microstructured optical fibers may enable an 8 dB suppression in the peak Brillouin gain coefficient compared to

acoustically homogeneous fibers. The large-mode-field area of the photonic crystal fiber can be combined with the acoustic suppression to yield an 18 dB combined suppression relative to standard telecommunications optical fibers, potentially enabling the amplification of kilowatt-level signals over a few meters of fiber or the transmission of watt-level signals over much longer distances.

ACKNOWLEDGMENTS

The authors wish to acknowledge the High Energy Laser Joint Technology Office for funding support. This work was supported in part by a grant of computer time from the DOD High Performance Computing Modernization (HPCMP) Program at the Air Force Research Laboratory DoD Supercomputing Resource Center. The authors thank Juan Carlos Chaves of the HPCMP Productivity Enhancement and Technology Transfer and Training team for programming support, and Thomas G. Ward, Jr. and Michael K. Shaffer for their assistance in reviewing the manuscript.

APPENDIX: DEFINITION OF THE FINITE ELEMENT VECTORS AND MATRICES

The definitions of the matrices **A**, **B**, **C**, and the vector **F** in (18) are included here for completeness. The shape function matrices $\mathbf{N}_k$,$\mathbf{N}_{xk}$,$\mathbf{N}_{yk}$, the Jacobian matrix $\mathbf{J}_k$, and the integration point weights W_k are defined as in Ref. 19 where k indexes the integration points. The square diagonal matrices $\mathbf{V}_L^2$ and $\mathbf{V}_T^2$ contain the longitudinal and shear acoustic velocities squared of each element in the diagonal entries. The vectors $\tilde{\mathbf{E}}_{ik}$ consist of the ith component of the electric field describing the fundamental optical mode of the fiber interpolated to integration point k within each element of the mesh using the hybrid element scheme.[25] We have used the symbol $\times$ to represent elementwise multiplication of vectors.

$$\mathbf{A}_{xx} \equiv \sum_{k=1}^{7} W_k \big[\mathbf{N}_{xk}^{\mathrm{T}} \cdot \mathbf{J}_k \cdot \mathbf{V}_L^2 \cdot \mathbf{N}_{xk} + \mathbf{N}_{yk}^{\mathrm{T}} \cdot \mathbf{J}_k \cdot \mathbf{V}_T^2 \cdot \mathbf{N}_{yk} + \beta^2 \mathbf{N}_k^{\mathrm{T}} \cdot \mathbf{J}_k \cdot \mathbf{V}_T^2 \cdot \mathbf{N}_k\big], \tag{A1}$$

$$\mathbf{A}_{xy} \equiv \sum_{k=1}^{7} W_k \left[\mathbf{N}_{yk}^{\mathrm{T}} \cdot \mathbf{J}_k \cdot \left(\mathbf{V}_L^2 - \mathbf{V}_T^2\right) \cdot \mathbf{N}_{xk}\right], \tag{A2}$$

$$\mathbf{A}_{xz} \equiv \sum_{k=1}^{7} W_k \left[i\beta \mathbf{N}_k^{\mathrm{T}} \cdot \mathbf{J}_k \cdot \left(\mathbf{V}_L^2 - \mathbf{V}_T^2\right) \cdot \mathbf{N}_{xk}\right], \tag{A3}$$

$$\mathbf{A}_{yy} \equiv \sum_{k=1}^{7} W_k \big[\mathbf{N}_{xk}^{\mathrm{T}} \cdot \mathbf{J}_k \cdot \mathbf{V}_T^2 \cdot \mathbf{N}_{xk} + \mathbf{N}_{yk}^{\mathrm{T}} \cdot \mathbf{J}_k \cdot \mathbf{V}_L^2 \cdot \mathbf{N}_{yk} + \beta^2 \mathbf{N}_k^{\mathrm{T}} \cdot \mathbf{J}_k \cdot \mathbf{V}_T^2 \cdot \mathbf{N}_k\big], \tag{A4}$$

$$\mathbf{A}_{yz} \equiv \sum_{k=1}^{7} W_k \left[i\beta \mathbf{N}_k^{\mathrm{T}} \cdot \mathbf{J}_k \cdot \left(\mathbf{V}_L^2 - \mathbf{V}_T^2\right) \cdot \mathbf{N}_{yk}\right], \tag{A5}$$

$$\mathbf{A}_{zz} \equiv \sum_{k=1}^{7} W_k \big[\mathbf{N}_{xk}^{\mathrm{T}} \cdot \mathbf{J}_k \cdot \mathbf{V}_T^2 \cdot \mathbf{N}_{xk} + \mathbf{N}_{yk}^{\mathrm{T}} \cdot \mathbf{J}_k \cdot \mathbf{V}_T^2 \cdot \mathbf{N}_{yk} + \beta^2 \mathbf{N}_k^{\mathrm{T}} \cdot \mathbf{J}_k \cdot \mathbf{V}_L^2 \cdot \mathbf{N}_k\big], \tag{A6}$$

$$\mathbf{B}_{xx} \equiv -\sum_{k=1}^{7} W_k \big[i\eta_{11} \mathbf{N}_{xk}^{\mathrm{T}} \cdot \mathbf{J}_k \cdot \mathbf{N}_{xk} + i\eta_{44} \mathbf{N}_{yk}^{\mathrm{T}} \cdot \mathbf{J}_k \cdot \mathbf{N}_{yk} + i\eta_{44}\beta^2 \mathbf{N}_k^{\mathrm{T}} \cdot \mathbf{J}_k \cdot \mathbf{N}_k\big], \tag{A7}$$

$$\mathbf{B}_{xy} \equiv -\sum_{k=1}^{7} W_k \left[i\left(\eta_{11} - \eta_{44}\right) \mathbf{N}_{yk}^{\mathrm{T}} \cdot \mathbf{J}_k \cdot \mathbf{N}_{xk}\right], \tag{A8}$$

$$\mathbf{B}_{xz} \equiv \sum_{k=1}^{7} W_k \left[\beta\left(\eta_{11} - \eta_{44}\right) \mathbf{N}_k^{\mathrm{T}} \cdot \mathbf{J}_k \cdot \mathbf{N}_{xk}\right], \tag{A9}$$

$$\mathbf{B}_{yy} \equiv -\sum_{k=1}^{7} W_k \big[i\eta_{44} \mathbf{N}_{xk}^{\mathrm{T}} \cdot \mathbf{J}_k \cdot \mathbf{N}_{xk} + i\eta_{11} \mathbf{N}_{yk}^{\mathrm{T}} \cdot \mathbf{J}_k \cdot \mathbf{N}_{yk} + i\eta_{44}\beta^2 \mathbf{N}_k^{\mathrm{T}} \cdot \mathbf{J}_k \cdot \mathbf{N}_k\big], \tag{A10}$$

$$\mathbf{B}_{yz} \equiv \sum_{k=1}^{7} W_k \left[\beta\left(\eta_{11} - \eta_{44}\right) \mathbf{N}_k^{\mathrm{T}} \cdot \mathbf{J}_k \cdot \mathbf{N}_{yk}\right], \tag{A11}$$

$$\mathbf{B}_{zz} \equiv -\sum_{k=1}^{7} W_k \big[i\eta_{44} \mathbf{N}_{xk}^{\mathrm{T}} \cdot \mathbf{J}_k \cdot \mathbf{N}_{xk} + i\eta_{44} \mathbf{N}_{yk}^{\mathrm{T}} \cdot \mathbf{J}_k \cdot \mathbf{N}_{yk} + i\eta_{11}\beta^2 \mathbf{N}_k^{\mathrm{T}} \cdot \mathbf{J}_k \cdot \mathbf{N}_k\big], \tag{A12}$$

$$\mathbf{C}_{xx} \equiv \mathbf{C}_{yy} \equiv \mathbf{C}_{zz} \equiv -\sum_{k=1}^{7} W_k \left[\mathbf{N}_k^{\mathrm{T}} \cdot \mathbf{J}_k \cdot \mathbf{N}_k\right], \tag{A13}$$

$$\mathbf{C}_{ij} = 0 \quad (i \neq j), \tag{A14}$$

$$\mathbf{F}_x \equiv \sum_{k=1}^{7} W_k \left\{2\gamma_{12}\mathrm{Re}\left[\tilde{\mathbf{E}}_{xk}^* \times \frac{\partial \tilde{\mathbf{E}}_{xk}}{\partial x} + \tilde{\mathbf{E}}_{yk}^* \times \frac{\partial \tilde{\mathbf{E}}_{yk}}{\partial x} + \tilde{\mathbf{E}}_{zk}^* \times \frac{\partial \tilde{\mathbf{E}}_{zk}}{\partial x}\right] + 2\gamma_{44}\left(2\mathrm{Re}\left[\tilde{\mathbf{E}}_{xk}^* \times \frac{\partial \tilde{\mathbf{E}}_{xk}}{\partial x}\right] + \frac{\partial \tilde{\mathbf{E}}_{xk}^*}{\partial y} \times \tilde{\mathbf{E}}_{yk} + \tilde{\mathbf{E}}_{xk}^* \times \frac{\partial \tilde{\mathbf{E}}_{yk}}{\partial y}\right)\right\} \cdot \mathbf{J}_k \cdot \mathbf{N}_k, \tag{A15}$$

$$\mathbf{F}_y \equiv \sum_{k=1}^{7} W_k \left\{2\gamma_{12}\mathrm{Re}\left[\tilde{\mathbf{E}}_{xk}^* \times \frac{\partial \tilde{\mathbf{E}}_{xk}}{\partial y} + \tilde{\mathbf{E}}_{yk}^* \times \frac{\partial \tilde{\mathbf{E}}_{yk}}{\partial y} + \tilde{\mathbf{E}}_{zk}^* \times \frac{\partial \tilde{\mathbf{E}}_{zk}}{\partial y}\right] + 2\gamma_{44}\left(2\mathrm{Re}\left[\tilde{\mathbf{E}}_{yk}^* \times \frac{\partial \tilde{\mathbf{E}}_{yk}}{\partial y}\right] + \frac{\partial \tilde{\mathbf{E}}_{xk}^*}{\partial x} \times \tilde{\mathbf{E}}_{yk} + \tilde{\mathbf{E}}_{xk}^* \times \frac{\partial \tilde{\mathbf{E}}_{yk}}{\partial x}\right)\right\} \cdot \mathbf{J}_k \cdot \mathbf{N}_k, \tag{A16}$$

$$\mathbf{F}_z \equiv \sum_{k=1}^{7} W_k \left[i\beta\gamma_{12}\left|\mathbf{E}_k\right|^2 + 2\gamma_{44}\left(i\beta\left|\mathbf{E}_{zk}\right|^2 + \frac{\partial \tilde{\mathbf{E}}_{xk}^*}{\partial x} \times \tilde{\mathbf{E}}_{zk} + \tilde{\mathbf{E}}_{xk}^* \times \frac{\partial \tilde{\mathbf{E}}_{zk}}{\partial x} + \frac{\partial \tilde{\mathbf{E}}_{yk}^*}{\partial y} \times \tilde{\mathbf{E}}_{zk} + \tilde{\mathbf{E}}_{yk}^* \times \frac{\partial \tilde{\mathbf{E}}_{zk}}{\partial y}\right)\right] \cdot \mathbf{J}_k \cdot \mathbf{N}_k. \tag{A17}$$

[1]R. Smith, Appl. Opt. **11**, 2489 (1972).
[2]E. Ippen and R. Stolen, Appl. Phys. Lett. **21**, 539 (1972).
[3]N. M. Kroll, J. Appl. Phys. **36**, 34 (1964).
[4]C. Tang, J. Appl. Phys. **37**, 2945 (1966).
[5]N. Shibata, K. Okamoto, and Y. Azuma, J. Opt. Soc. Am. B **6**, 1167 (1989).
[6]R. W. Boyd, K. Rzazewski, and P. Narum, Phys. Rev. A **42**, 5514 (1990).
[7]A. Kobyakov, M. Sauer, and D. Chowdhury, Adv. Opt. Photon. **2**, 1 (2010).
[8]J. E. Rothenberg, P. A. Thielen, M. Wickham, and C. P. Asman, in *Fiber Lasers V: Technology, systems, and Applications*, edited by J. Broeng and C. Headley, Proc. SPIE Vol. 6873 (SPIE, Bellingham, WA, 2008), pp. 68730O-1–68730O-7.
[9]V. I. Kovalev and R. G. Harrison, Opt. Lett. **31**, 161 (2006).
[10]P. Dragic, C.-H. Liu, G. C. Papen, and A. Galvanauskas, in *Proceedings of the Conference on Lasers and Electro-Optics/Quantum Electronics and Laser Science and Photonic Applications Systems Technologies* (Optical Society of America, 2005), Vol. 3, pp. 1984–1986.
[11]M.-J. Li, X. Chen, J. Wang, S. Gray, A. Liu, J. A. Demeritt, A. B. Ruffin, A. M. Crowley, D. T. Walton, and L. A. Zenteno, Opt. Express **15**, 8290 (2007).
[12]F. Poletti, K. Furusawa, Z. Yusoff, N. Broderick, and D. Richardson, J. Opt. Soc. Am. B **24**, 2185 (2007).
[13]V. Laude, A. Khelif, S. Benchabane, M. Wilm, T. Sylvestre, B. Kibler, A. Mussot, J. M. Dudley, and H. Maillotte, Phys. Rev. B **71**, 045107 (2005).
[14]P. Dainese, P. S. J. Russell, N. Joly, J. C. Knight, G. S. Wiederhecker, H. L. Fragnito, V. Laude, and A. Khelif, Nature Phys. **2**, 388 (2006).
[15]K. Furusawa, Z. Yusoff, T. Monro, N. Broderick, and D. Richardson, Opt. Lett. **31**, 2541 (2006).
[16]J.-C. Beugnot, T. Sylvestre, D. Alasia, H. Maillotte, V. Laude, A. Monteville, L. Provino, N. Traynor, S. F. Mafang, and L. Thevenaz, Opt. Express **15**, 15517 (2007).
[17]G. P. Agrawal, *Nonlinear Fiber Optics* 3rd ed. (Academic, New York, 2001).
[18]J. B. Spring and B. G. Ward, Opt. Lett. **35**, 31 (2010).
[19]B. G. Ward and J. B. Spring, Opt. Express **17**, 15685 (2009).
[20]A. H. McCurdy, J. Lightwave Technol. **23**, 3509 (2005).
[21]J. F. Nye, *Physical Properties of Crystals, Their Representation by Tensors and Matrices* (Clarendon, Oxford, 1985).
[22]E. Peral and A. Yariv, IEEE J. Quantum Electron. **35**, 1185 (1999).
[23]A. D. Berk, IRE Trans. Antennas Propag. **4**, 104 (1956).
[24]R. P. Feynman, R. B. Leighton, and M. Sands, *The Feynman Lectures on Physics* (Addison-Wesley, Reading, MA, 1977), Vol. II, Chap. 19.
[25]M. Koshiba and Y. Tsuji, J. Lightwave Technol. **18**, 737 (2000).
[26]H. Goldstein, *Classical Mechanics* (Addison-Wesley, Reading, MA, 1950).
[27]R. W. Boyd, *Nonlinear Optics* (Academic, New York, 1992).
[28]P. Dragic, J. Opt. Soc. Am. B **26**, 1614 (2009).
[29]F. D. Teodoro and C. D. Brooks, Opt. Lett. **30**, 2694 (2005).
[30]V. I. Kovalev and R. G. Harrison, Opt. Lett. **27**, 2022 (2002).